JTTEE5 11:536-541
© ASM International

Peer Reviewed

A Comparison of the Corrosion Behavior of WC-Co-Cr and WC-Co HVOF Thermally Sprayed Coatings by In Situ Atomic Force Microscopy (AFM)

Joan M. Perry, Anne Neville, and Trevor Hodgkiess

(Submitted 13 March 2001; in revised form 15 June 2001)

The corrosion behavior of WC-Co-Cr and WC-Co high velocity oxygen fuel (HVOF) sprayed coatings were examined in static saline conditions. Direct current (DC) polarization tests were conducted and the electrochemical corrosion behavior was shown, by in situ atomic force microscopy (AFM) and scanning electron microscopy (SEM), to be complex because of the composite ceramic-metal nature of the coating. The addition of chromium to the matrix greatly enhanced the corrosion resistance of the coating.

Keywords atomic force microscopy (AFM), cermet, corrosion, electrochemical

1. Introduction

Thermally sprayed coatings are now used extensively in a variety of applications.[1-4] However, their application has often preceded detailed knowledge or understanding of their corrosion mechanisms or rates. Previous studies involving plasma sprayed coatings[5,6] have shown that good quality coatings, in terms of low porosity, are essential to protect the substrate from corrosion. There are many thermal spray processes available to date: the high velocity oxygen fuel (HVOF) process, which uses higher exhaust velocities and lower flame temperatures than other processes, can produce coatings of low porosity levels (1%) and avoids alteration of the mechanical properties of the substrate.[7]

The corrosion characteristics of thermal sprayed coatings in static saline environments are extremely important where the flow of aqueous solution over components intermittently ceases. The multiphased structure of these coatings (hard ceramic particles encased in a metallic binder) induces complex corrosion behavior as shown in recent work.[8-10] It has been established[11,12] that where coatings are applied by a high-quality process and under stringent quality control procedures, the coatings can provide a very effective barrier to the substrate and prevent any corrosion from occurring. In this situation, however, it is very important to appreciate that corrosion of the coating can occur and that initiation and propagation of corrosion, associated with microstructural features of the composite system, are a real issue. For improvements to the coating corrosion resistance to be made, a full understanding of the corrosion rates and mechanisms, and in particular the resistance of the metallic binder (in cermet systems), is required. In addition, an understanding of static corrosion behavior can help reveal the mechanisms of the coating degradation in erosion-corrosion environments.[13,14]

This article investigates the corrosion rates and mechanisms of two HVOF coatings (WC-Co-Cr and WC-Co).

Joan M. Perry and **Trevor Hodgkiess,** Department of Mechanical Engineering, University of Glasgow, Glasgow, Scotland, G12 8QQ; and **Anne Neville,** Department of Mechanical and Chemical Engineering, Heriot-Watt University, Edinburgh, Scotland EH14 4AS. Contact e-mail: a.neville@hw.ac.uk.

2. Experimental

Two HVOF sprayed coatings are studied in this work: a WC-Co-Cr coating with nominal composition 86%WC-10%Co-4%Cr, and a WC-Co coating with a nominal composition 86%WC-14%Co. The coatings were applied to a stainless steel substrate (UNS S31603). Specimens were soldered on the rear side to an electrical conducting wire and subsequently encapsulated in nonconducting resin. The exposed coated face of the specimen was then ground with silicon carbide abrasive papers and polished to a 6 μm diamond finish.

Static corrosion experiments were carried out on samples with an exposed area of 1 cm^2 in artificial seawater (Instant Ocean, Phillip Harris, UK) dissolved in distilled water to yield a salinity of 35 000 ppm. The main seawater constituents were 19 300 ppm chloride, 11 000 ppm sodium, 2700 ppm sulfate, 1300 magnesium, 400 ppm calcium, 400 ppm potassium, and 150 ppm bicarbonate ions. The specimen-resin interfaces were sealed using Lacomit varnish (Agar Aids, UK) to prevent interference from the substrate. Electrochemical monitoring was carried out with a standard three-electrode cell, comprising a platinum auxiliary electrode and a saturated calomel reference electrode (SCE). Direct current (DC) anodic polarization tests were carried out after 1 h immersion in the seawater at 18 and 50 °C. The seawater was left open to the atmosphere. The potentiostat was used to scan the electrode potential of the coating samples from the free corrosion potential (E_{corr}) in the positive (anodic) direction until a current in the range of 500-700 μA/cm^2

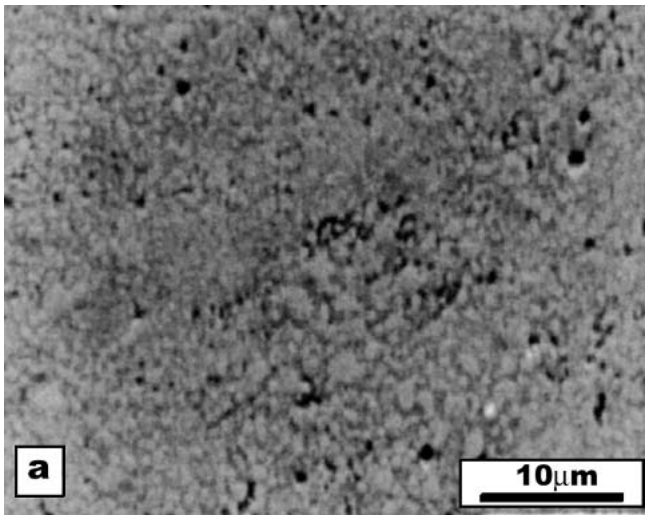

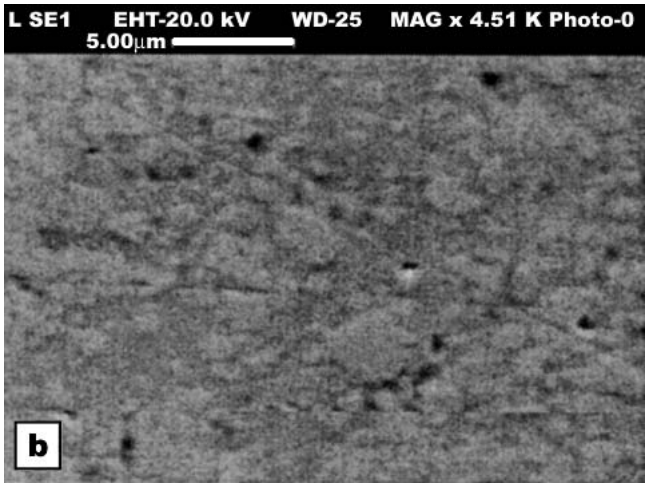

Fig. 1 Polished section of the HVOF sprayed coatings prior to corrosion testing: **(a)** WC-Co-Cr and **(b)** WC-Co

Table 1 EDX Measurements on the WC-Co-Cr and WC-Co Coatings Prior to Corrosion Testing

	wt.%	
Element	**WC-Co-Cr**	**WC-Co**
W	83-85	87-88
Co	9-11	12-13
Cr	3-5	Nil

was reached. The scan rate used was 15 mV/min. Each test was repeated three times and good reproducibility in the form of the polarization curve was obtained. Representative figures are presented in the Results section and values for corrosion rates are the range of values obtained.

In addition, an atomic force microscope (AFM) was used to map the topography of the coatings during accelerated corrosion tests. The AFM was configured to probe the surface under water and record images during anodic polarization tests. Each image took 6 min to produce, during which time the potential had shifted by approximately 90 mV.

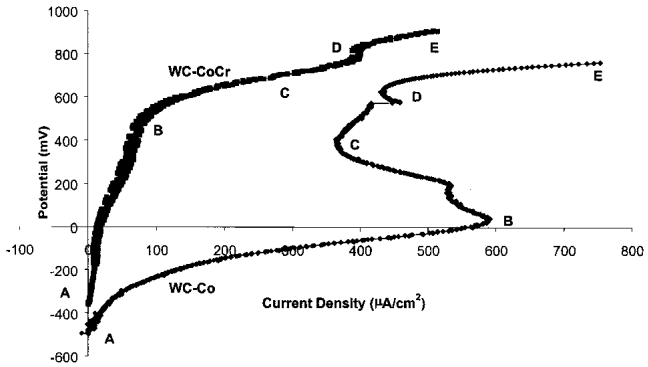

Fig. 2 Anodic polarization curves in static artificial seawater at 18 °C on WC-Co-Cr and WC-Co HVOF sprayed coatings

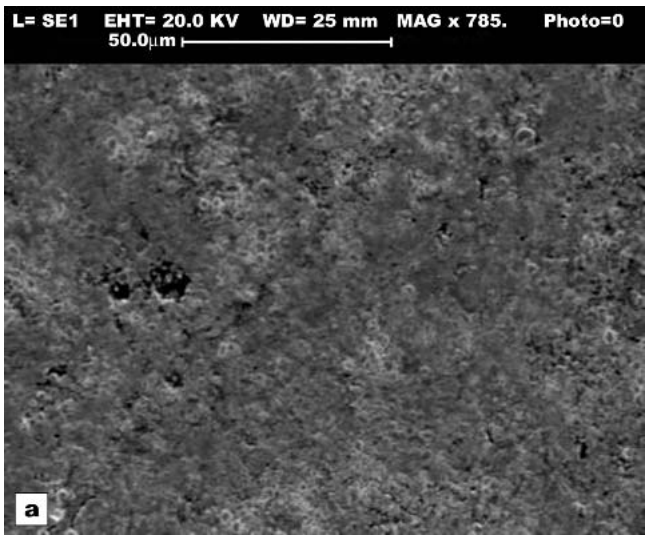

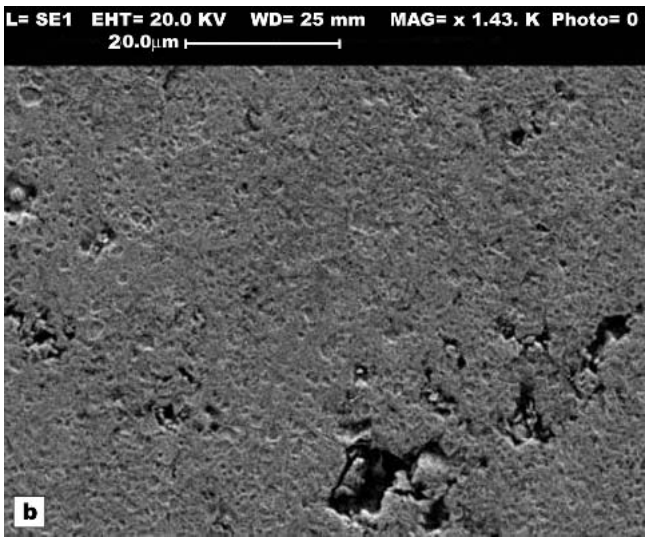

Fig. 3 Corrosion attack on the surface of **(a)** WC-Co and **(b)** WC-Co-Cr HVOF sprayed coatings after anodic polarization in static artificial seawater at 18 °C

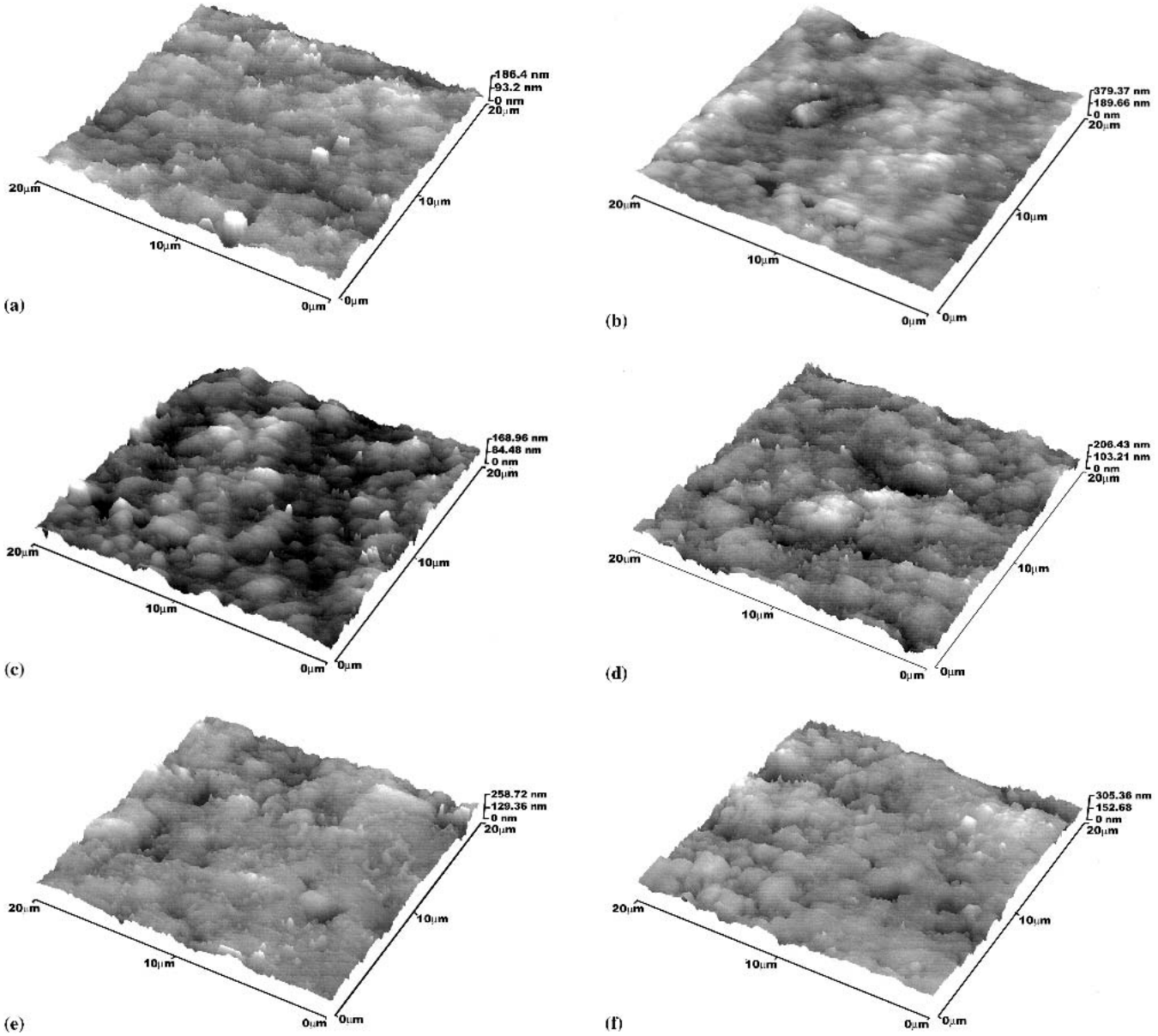

Fig. 4 In situ AFM images corresponding to the anodic polarization scan conducted on WC-Co coating shown in Fig. 2. **(a)** Polished coating prior to polarization; **(b)** points A to B; **(c)** points B to C; **(d)** points C to D; **(e)** points D to E; and **(f)** end of anodic polarization

Microstructural examination of the as-received coatings and specimens after corrosion tests were performed using a scanning electron microscope (SEM). Chemical analysis was performed with the energy dispersive x-ray (EDX) attachment on the SEM. X-ray diffraction (XRD) measurements were taken on the as-received coatings.

3. Characterization

Figure 1(a) and (b) shows polished sections of the WC-Co-Cr and WC-Co coatings, respectively. The micrographs show the blocky tungsten-carbide particles, with typical sizes of <5 μm, encased within a metallic matrix. An average analysis carried out by EDX on a 30 × 30 μm area gave the compositions shown in Table 1. Analysis by XRD showed limited decarburization on both coatings revealed by the presence of small W_2C peaks on the XRD spectra.

4. Results

Figure 2 shows the anodic polarization response of both coatings after immersion in artificial seawater for 1 h at 18 °C. The WC-Co coating has a very complex electrochemical response. Initially, it shows behavior akin to active corrosion behavior because the current rapidly rises with potential. When the current is in excess of 500 μA/cm^2 (around 0 mV as determined by SCE),

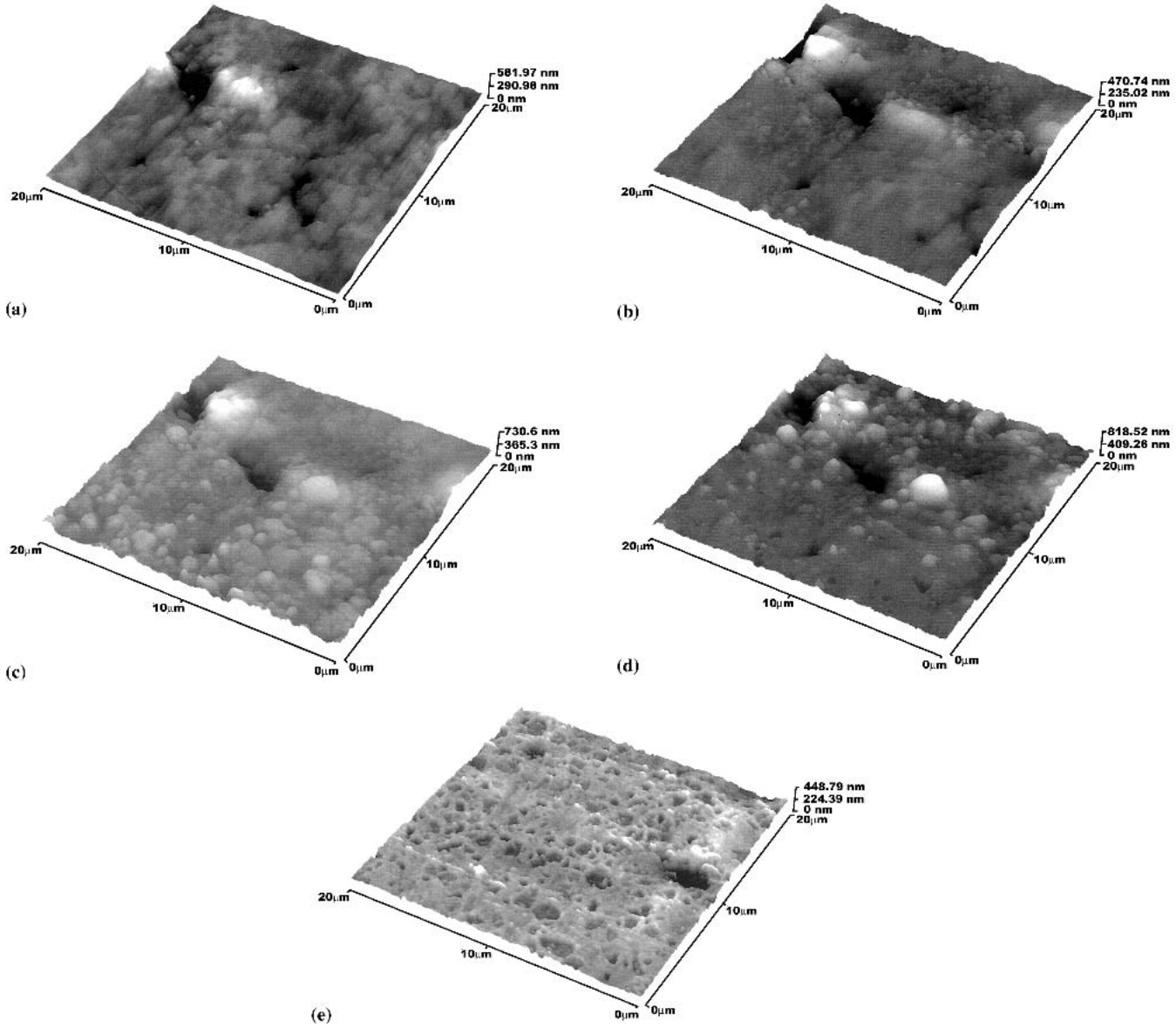

Fig. 5 In situ AFM images corresponding to the anodic polarization scan conducted on WC-Co-Cr coating shown in Fig. 2. **(a)** Polished coating prior to polarization; **(b)** point B; **(c)** point C; **(d)** point D; and **(e)** end of anodic polarization

the current decreases with increasing potential until a potential of +400 mV (SCE), when the current again increases with increasing potential. In contrast, the WC-Co-Cr coating displays lower currents as a function of increasing potential, more akin to passive corrosion behavior. The current increases, but more slowly than for the WC-Co coating, until a first breakdown potential at approximately +500 mV (SCE) and a second breakdown potential at +800 mV (SCE). Examination of the specimens after anodic polarization by SEM revealed differing corrosion mechanisms on the two coatings. Figure 3(a) shows the WC-Co coating, where the matrix has been attacked, quite severely in some areas, and some crevice corrosion is visible between the hard phase and matrix. The matrix on the WC-Co-Cr coating appears to have little corrosion damage but the hard phase particles have been removed (Fig. 3b).

Further investigation of the progression of corrosive attack as a function of applied potential, at 18 °C, on both coatings was monitored with the AFM. The three-dimensional (3D) images cover an area of 20 × 20 μm. The initial scan of the WC-Co coating at the free corrosion potential (Fig. 4a) shows the surface of the polished coating with slight spikes caused by polishing effects. As the potential is scanned more positive to point B on the WC-Co curve in Fig. 2, the surface is smoothed and extensive matrix dissolution has occurred, showing clearly the hard phase particles (Fig. 4b). During the decrease in current (points B to C), the matrix is dissolving at a steady rate, defining the hard phase particles more clearly (Fig. 4c). As the current increases (points C to D in Fig. 4d), the matrix dissolves further, revealing the smaller hard phases from point D to E (Fig. 4e). At the end of the anodic polarization, areas where the matrix has dissolved in

some regions and areas of attack around the matrix-hard phase interface can be seen (Fig. 4f).

In a similar manner, the corrosion mechanisms during anodic polarization of the WC-Co-Cr coating were examined. Figure 5(a) shows the coating at the free corrosion potential with the light grey hard phases encased in the darker grey matrix. Because the potential is scanned more positive than E_{corr} to point B on the WC-Co-Cr curve in Fig. 2, the smaller hard phase particles are more pronounced (Fig. 5b). The rapid increase in current with the potential corresponds to dramatic matrix dissolution and leaves the hard phase protruding from the matrix (Fig. 5c). As the current stabilizes at point D, carbides begin to fall out from the matrix and leave voids behind (Fig. 5d). This progresses until the end of the scan at point E, where the matrix consists mainly of voids left by the carbide particles and a few carbides on the next layer are visible (Fig. 5e).

After immersion in seawater for 1 h at 50 °C, the kinetics of the anodic polarization processes are accentuated on both coatings. Figure 6 shows that both coatings display higher corrosion currents than at 18 °C as the potential is scanned more positive from E_{corr}. WC-Co-Cr, as at 18 °C, shows a lower corrosion rate than the WC-Co coating. The corrosion mechanism on the WC-Co coating is extensive general attack on the surface (Fig. 7a), which leaves the hard phases standing out from the matrix. The WC-Co-Cr coating has areas of more localized attack (Fig. 7b), which are superimposed on the type of attack shown at 18 °C, and lead to general loss of carbides. Table 2 summarizes the corrosion rates, determined by Tafel extrapolation, of the coatings at the two temperatures. Each test was replicated three times and the region in excess of 30 mV away from the corrosion potential exhibited good linearity. Only the anodic portion was used because in previous tests good agreement was found between the values extrapolated from anodic and cathodic data. The corrosion rate of the WC-Co coating is greater than the WC-Co-Cr coating at both 18 and 50 °C, but more significantly at 50 °C.

5. Discussion

Many of the static corrosion studies already carried out on WC-Co-Cr coatings have focused on the mechanism of corrosive attack and have not included measurement of the actual corrosion rates. This study includes this detail and highlights the better static corrosion resistance of the Co-Cr matrix over the Co matrix, which has been documented elsewhere in erosion-corrosion studies.[15,16]

It can be deduced, and indeed was observed in this study, that the corrosion process in the first instance is concentrated mainly on the binder phases. The two binder phases (Co and Co-Cr) have resulted in two differing corrosion mechanisms for the coatings. At 18 °C, the Co-Cr binder corrodes at the carbide-matrix interfaces uniformly over the coating surface and eventually extensive hard phase removal occurs (Fig. 5). The Co binder has more general areas of uniform matrix dissolution (Fig. 4), which leaves the carbide particles standing out from the surface. At 50 °C, the attack on the Co-Cr matrix is essentially the same as at 18 °C with additional localized regions of deep corrosion (Fig. 7b) where the removal of the matrix has resulted in unsupported hard phases.

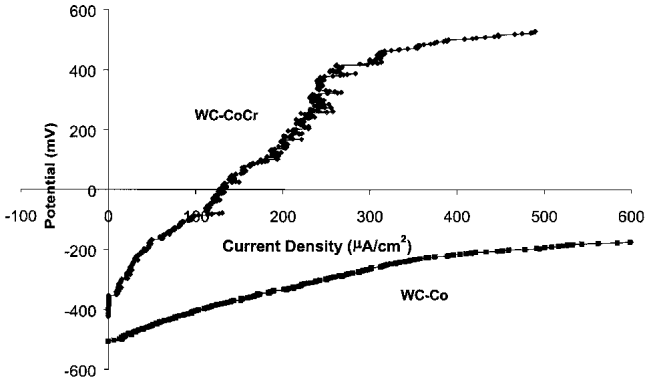

Fig. 6 Anodic polarization curves at 50 °C in static seawater on WC-Co-Cr and WC-Co coatings

The electrochemical behavior has been shown to be complex, especially on WC-Co. By linking the observations from microscopy with the electrochemical response, we deduced that the decrease in current experienced at point B in Fig. 2 is most probably due to the reduction in available area of matrix for corrosion once it is preferentially dissolved from the upper coating layer. The reduction in current is similar to the active-passive transition exhibited on many passive alloys, but the main distinction is that the current in this material is not reduced to passive values after the peak at B.

The addition of Cr to the Co matrix obviously has a profound effect on the corrosion resistance of the coating. It is well documented and understood through studies on the effect of Cr additions in high-grade alloys[17] that Cr is the key element for forming a passive film. In this work, the binder alloy is essentially a 29%Cr-Co-based alloy, and alloys similar to this composition have been shown to exhibit passivity in static saline solutions.[18] One potential explanation for the difference between the corrosion mechanisms on the WC-Co-Cr and WC-Co coatings is the susceptibility of the passive type matrix (Co-Cr) to localized corrosion on a microscale, which mimics the crevice corrosion mechanism often reported on stainless steels and other passive alloys in saline solutions (see Ref. 19). This corrosion, as confirmed by microscopy, is prevalent at the occluded regions of the carbide-matrix boundaries and proceeds at a slower rate than the general corrosion of the Co matrix.

Another factor that could influence the level of corrosion attack on the matrix is the difference in electrode potential of the major coating constituents (WC and matrix). The free corrosion potential of the WC-Co coating shows consistently more electronegative values than the WC-Co-Cr coating. Given that the free corrosion potential of the coating is a composite value from the hard phase and matrix, it is reasonable to assume that the Co component is more electronegative than the Co-Cr matrix. As such, there will be a larger driving force for micro-galvanic corrosion and this may partially account for the increased corrosion attack on the WC-Co cermet.

6. Conclusions

The use of an AFM can aid the determination of corrosion mechanisms on a microscale.

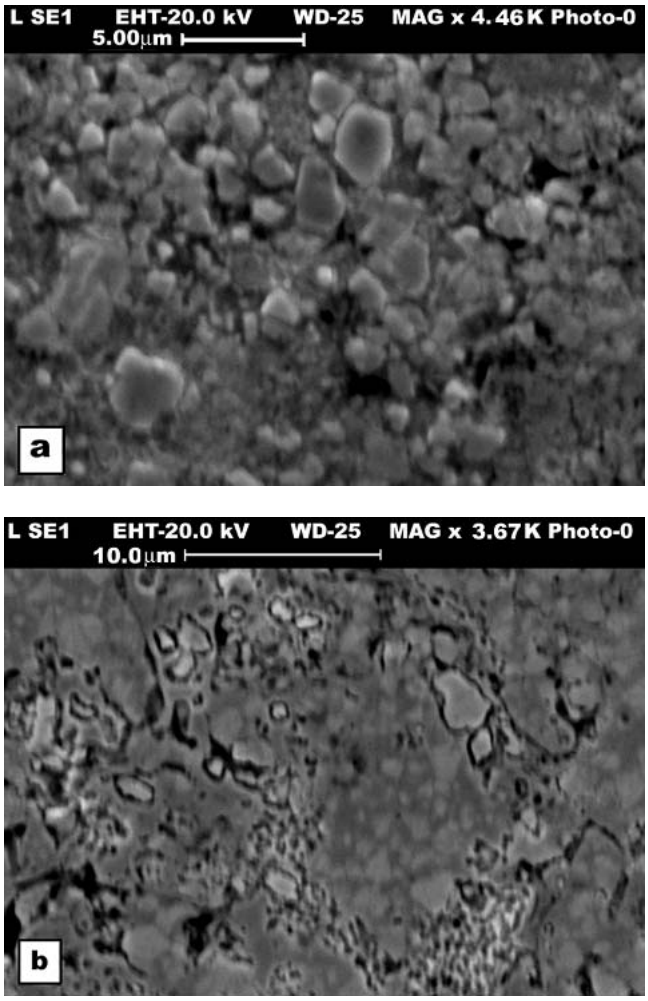

Fig. 7 Corrosion attack on the surface of **(a)** WC-Co and **(b)** WC-Co-Cr HVOF sprayed coatings after anodic polarization in static artificial seawater at 50 °C

Table 2 Corrosion Current Densities of the Two Coatings Determined by Tafel Extrapolation of Anodic Polarization Data

	I_{corr}, μA/cm²	
Coating	**18 °C**	**50 °C**
WC-Co	9-11	16
WC-Co-Cr	3-9	10-12

The addition of chromium to a cobalt matrix increases the corrosion resistance of a WC-based HVOF sprayed cermet coating and the extent of this has been quantified.

Although the WC-Co-Cr coating suffers from more localized attack at 18 °C, accentuated at the hard phase-matrix interface, the WC-Co has more uniform corrosion affecting the entire matrix.

An increase in temperature results in extensive dissolution of the cobalt matrix, whereas on the CoCr matrix more severe attack is further localized in regions not associated with any specific microstructural features.

References

1. S.T. Tsai and H.C. Shih: "The Use of Thermal-Spray Coatings for Preventing Wet H_2S Cracking in HSLA Steel Plates," *Corros. Prev. Control,* 1997, *44,* pp. 42-48.
2. R.J. Duncan and C.B. Thompson: "A Guide to Weld and Thermal Spray Hardfacing in the Pulp and Paper Industry. Part 2: Applications," *Mater. Des.,* 1991, *11,* pp. 71-75.
3. C.B. Thompson and A. Garner: "Identification and Control of Wear in the Pulp and Paper Industry," *Pulp Paper Can.,* 1986, *87,* pp. 53-56.
4. L. Pejryd, J. Wigren, D.J. Greving, J.R. Shadley, and E.F. Rybicki: "Residual Stresses as a Factor in the Selection of Tungsten Carbide Coatings for a Jet Engine Application," *J. Therm. Spray Technol.,* 1995, *4,* pp. 268-74.
5. A.A. Ashary and R.C. Tucker: "Electrochemical Corrosion Studies of Alloys Plasma Sprayed With Cr_2O_3," *Surf. Coat. Technol.,* 1989, *39/40,* pp. 701-09.
6. A.A. Ashary and R.C. Tucker: "Electrochemical and Longterm Corrosion Studies of Several Alloys in Bare Condition and Plasma Sprayed with Cr_2O_3," *Surf. Coat. Technol.,* 1990, *43/44,* pp. 567-76.
7. L. Pawlowski: *The Science and Engineering of Thermal Spray Coatings,* John Wiley and Sons, New York, 1994.
8. J.M. Perry, A. Neville, V. Wilson, and T. Hodgkiess: "Assessment of the Corrosion Rates and Mechanisms of a WC-Co-Cr HVOF Coating in Static and Liquid-Solid Impingement Saline Environment," *Surf. Coat. Technol.,* 2001, *137,* p. 43.
9. A. Neville and T. Hodgkiess: "Corrosion Behavior and Microstructure of Two Thermal Spray Cermet Coatings," *Surf. Eng.,* 1996, *12,* pp. 303-12.
10. J.M. Guilemany, J. Fernandez, J.M. de Paco, and J. Sanchez: "Corrosion Resistance of HVOF WC-Co and TiC/Ni-Ti Coatings Sprayed on Commercial Steel," *Surf. Eng.,* 1998, *14,* pp. 133-35.
11. R. Hoffman, M.P.W. Vreijling, G.M. Ferrari, and J.H.W. de Wit: "Electrochemical Methods for Characterization of Thermal Spray Corrosion Resistant Stainless Steel Coatings," *Mater. Sci. Forum,* 1998, *280-292,* pp. 641-54.
12. A. Neville and T. Hodgkiess: "An Analysis of Environmental Factors Affecting Corrosion Behavior of Thermal Spray Cermet Coatings" in *Proceedings of the 15th International Thermal Spray Conference*, 1998, ASM, pp. 161-66.
13. T. Hodgkiess, A. Neville, and S. Shrestha: "Electrochemical and Mechanical Interactions During Erosion-Corrosion of a High Velocity Oxy-Fuel Coating and a Stainless Steel," *Wear,* 1999, *233-235,* pp. 623-34.
14. S. Shrestha, A. Neville, and T. Hodgkiess: "The Effect of Post-Treatment of a High-Velocity Oxy-Fuel Ni-Cr-Si-B Coating, Part I: Microstructure/Corrosion Behavior Relationships," *J. Therm. Spray Technol.*, 2001, *10*(3), pp. 470-79.
15. M. Bjordal, E. Bardal, T. Rogne, and T.G. Eggen: "Erosion and Corrosion Properties of WC-Coatings and Duplex Stainless Steel in Sand Containing Seawater," *Wear,* 1995, *186-187,* pp. 508-14.
16. T. Rogne, T. Solem, and J. Berger: "Effect of Composition and Corrosion Properties of the Metallic Matrix on the Erosion-Corrosion Behavior of HVOF Sprayed WC-Coatings" in *Corrosion '98,* Paper No. 495, National Association of Corrosion Engineers (NACE), Houston, TX, 1998.
17. M. Bjordal, E. Bardal, T. Rogne, and T.G. Eggen: "Combined Erosion and Corrosion of Thermal Sprayed WC and CrC Coatings," *Surf. Coat. Technol.,* 1995, *70*(2-3), pp. 215-20.
18. A. Neville, M. Reyes, T. Hodgkiess, and A. Gledhill: "Mechanisms of Wear on a Co-Base Alloy in Liquid–Solid Slurries," *Wear,* 2000, *238,* pp. 138-50.